European Journal of Cell Biology 102 (2023) 151346

Contents lists available at ScienceDirect

European Journal of Cell Biology

journal homepage: www.elsevier.com/locate/ejcb

Ozone mediates the anticancer effect of air plasma by triggering oxidative cell death caused by H_2O_2 and iron

Manami Suzuki-Karasaki [a,b], Yushi Ochiai [a], Shizuka Innami [a], Hiroshi Okajima [c], Miki Suzuki-Karasaki [a], Hideki Nakayama [d], Yoshihiro Suzuki-Karasaki [a,*]

[a] Department of Research and Development, Plasma ChemiBio Laboratory, Nasushiobara, Tochigi, Japan
[b] Graduate School of Medical Sciences, Kumamoto University, Kumamoto, Japan
[c] Communication&Control Systems Company, Tokyo Keiki Incorporation, Tokyo, Japan
[d] Department of Oral and Maxillofacial Surgery, Faculty of Life Sciences, Kumamoto University, Kumamoto, Japan

ARTICLE INFO

Keywords:
Cancer, ozone
Tumor-specificity
Monopolar perinuclear mitochondrial clustering
Cold atmospheric plasma
Plasma-activated medium

ABSTRACT

Cold atmospheric plasmas and plasma-treated solutions (PTSs) have emerged as promising approaches in cancer treatment because of their tumor-selective actions. While oxidative stress is critical for their effects, the precise mechanisms, including chemical mediators, remain obscure. Previously, we reported that air plasma-activated medium (APAM) exhibited tumor-selective anticancer activity. The fragmentation of mitochondria and their asymmetrical assembly around the peripheral regions of the damaged nucleus, namely, monopolar perinuclear mitochondrial clustering (MPMC), proceed to the effect. Subsequently, we found that APAM had a substantial amount of O_3 in addition to hydrogen peroxide (H_2O_2), nitrile (NO_2), and nitrate (NO_3^-). In the present study, we investigated the possible role of O_3 in the anticancer effect. For this purpose, we created a nitrogen oxide-free ozonated medium ODM. ODM exhibited potent cytotoxicity against various cancer but not nonmalignant cells. ODM also increased MPMC, hydroxyl radicals, lipid peroxides, and their shifts to perinuclear sites in cancer cells. Catalase and iron chelation prevented these events and cytotoxicity. ODM also decreases the intracellular labile irons while increasing those within mitochondria. ODM had substantial H_2O_2, but this oxidant failed to cause MPMC and cytotoxicity. These results show that ODM can mimic the effects of APAM, including MPMC and tumor-selective anticancer effects. The findings suggest that O_3 is critical in mediating the anticancer effects of APAM by triggering oxidative cell death caused by H_2O_2 and iron.

1. Introduction

Cold atmospheric plasmas (CAPs) are partially ionized gases containing ions, electrons, and free radicals and have tumor-selective cytotoxicity. CAP flushing into various solutions, such as culture media, buffers, and infusion fluids, results in plasma-treated solutions (PTSs). They also preferentially injure tumor cells while minimally damaging nonmalignant cells (Keidar et al., 2012; Yan et al., 2018; Ando et al., 2021). CAPs and PTSs also reduce tumor growth in animal models with minimal adverse events. These effects of CAP-based treatments have attracted considerable attention for cancer treatment. However, PTSs have different chemical and biological properties depending on the physical nature of the generated plasmas, the solutions used, and various experimental parameters. In addition, biological outcomes may vary significantly, depending on the target cell system. As a result, their actions are highly complicated. While most of them induce apoptosis, some can trigger nonapoptotic cell death forms, including autophagy (Ito et al., 2018; Yoshikawa et al., 2020), necroptosis (Ando et al., 2021),

Abbreviations: APAM, air plasma-activated medium; 3-AT, 3-amino-1,2,4-Triazole; BP, 2,2′-Bipyridyl; CAPs, cold atmospheric plasmas; DFO, Deferoxamine; Drp, dynamin-related protein; ER, endoplasmic reticulum; Fer-1, Ferrostatin-1, FeR, FeRhoNox™-1; FO, FerroOrange; GA, Golgi apparatus; HDF, human dermal fibroblasts; hFOB, human fetal osteoblasts; Hoe, Hoechst 33342; Hydrop, HYDROP™; LipRG, LipiRADICAL Green; LIPs, labile iron pools; LPO, lipid peroxide; MitoSOX, MitoSOX™ Red CMXRos; MPMC, monopolar perinuclear mitochondrial clustering; mROS, mitochondrial reactive oxygen species; MTFG, Mito-FerroGreen; MTR, MitoTracker Red; NC, Nocodazole; OC, oral cancer; ODM, ozone-dissolved medium; OXO, OxiORANGE™; PNMC, perinuclear mitochondrial clustering; PTSs, Plasma-treated solutions; ROS/RNS, reactive oxygen/nitrogen species; TTG, tubulin tracker green.

* Corresponding author.
E-mail address: suzuki.pcbl@gmail.com (Y. Suzuki-Karasaki).

https://doi.org/10.1016/j.ejcb.2023.151346
Received 25 April 2023; Received in revised form 1 July 2023; Accepted 2 August 2023
Available online 3 August 2023

and ferroptosis (Jo et al., 2022) in various cancer cell models. Although numerous reports have shown the vital role of reactive oxygen and nitrogen species (ROS/RNS) in mediating antitumor effects, the detailed mechanisms remain obscure. Moreover, CAPs have complicated components, and the complete chemical identification of their active substances is challenging. Indeed, many kinds of chemical species are found, including atomic oxygen, singlet oxygen, superoxide ($O_2^{\bullet-}$), hydroxyl radicals($^{\bullet}OH$), hydrogen peroxide (H_2O_2), nitric oxide (NO), and other nitrogen oxides (NOx). Different PTSs have two long-lived oxidants, H_2O_2, and NOx products, nitrite (NO_2^-) and nitrate (NO_3^-), which are considered to mediate the effect. More complicatedly, the exact contents of these species vary considerably depending on the CAP source, settings, and ambient conditions. In addition, multiple oxidants can function cooperatively. Several studies have shown the synergistic effect of H_2O_2 and NO_2^- in apoptosis (Girard et al., 2016; Bauer, 2019). Consequently, the primary mediator(s) and their molecular targets in the antitumor properties are poorly understood. Such chemical ambiguity heavily frustrates distinct descriptions of the mechanism of action and clinical applications.

O_3 is an oxygen allotrope that consists of three oxygen atoms. It is an acrid gas at the standard temperature and pressure. O_3 is an unstable molecule with unique physicochemical and biological properties owing to its resonance structures. It has the second-highest oxidizing power after fluorine. O_3 directly injures the bacterial cell membrane by oxidizing phospholipids and lipoproteins and has potent antibacterial activity. O_3 also inactivates viruses, fungi, yeasts, and protozoa. Therefore, they are widely used for sterilization and disinfection. O_3 has also been used to treat various diseases for over a century (Baeza-Noci and Pinto-Bonilla, 2021). Moreover, numerous in vitro and in vivo studies and a few clinical trials (Bocci, 2006; Clavo et al., 2018) have shown the anticancer effects of O_3. O_3 has a direct antitumor effect in some cancers. It also has indirect effects, such as immunomodulatory, synergistic, or adjuvant effects with various anticancer drugs (cisplatin, 5-fluorouracil, etoposide, and gemcitabine) and radiation (Zänker and Kroczek, 1990; Cannizzaro et al., 2007; Simonetti et al., 2017). O_3 is administered to animals in different ways, including topical gas, rectal or intraperitoneal insufflation, and intravenous or intratumoral injection. O_3 has a substantial solubility in water (14 mmol/L at 20 °C) and has also been used as ozonated water or medium. However, it must be aware that pure O_3 production by conventional methods is challenging. The most widely used method to generate O_3 is the silent discharge in the air. However, in addition to molecular oxygen (O_2), this method results in the simultaneous excitation of molecular nitrogen (N_2), leading to the production of various NOx. Accordingly, O_3 made by standard methods could contain NOx, such as NO and nitric dioxide, producing chemically more stable NO_2^- and NO_3^- in ozonated fluids. NOx can produce O_3 and more complicated, harmful oxidants in the presence of light. In addition, NO has been recognized as a primary modulator of cell death and a potential target for anticancer therapy (Kamm et al., 2019; Kim and Thomas, 2022). As a result, the co-existence of bystander NOx could interfere with the precise evaluation of the biological activity of O_3 in these ozonated fluids. Thus, eliminating NOx is essential to define the effect of O_3 itself. Moreover, compared with gaseous O_3, much less is known about the underlying mechanisms of the antitumor activity of O_3 in solutions.

Mitochondria are highly plastic, dynamic, and heterogenous organelles in connection with diverse functions. Their size, shape , and location vary in different tissues, cells, and experimental conditions. An emerging view is that mitochondrial shape and location changes are not passive events. Instead, they are active events coupled with cellular functions, cell death, and survival (Twig and Shirihai, 2011; Hoppins and Nunnari, 2012; Pendin et al., 2017). Mitochondria can distribute broadly throughout the cytoplasm (Pan-cytoplasmic), subplasmalemmal, or perinuclear sites. Pan-cytoplasmic distribution governs Ca^{2+} transport from the endoplasmic reticulum (ER) via tethering with ER (Pedriali et al., 2017). The subplasmalemmal distribution controls Ca^{2+} channel activity by regulating mitochondrial function as a Ca^{2+} reservoir (Quintana et al., 2006). The mitochondrial location around the perinuclear regions is called perinuclear mitochondrial clustering (PNMC). This response is induced by stresses, such as hypoxia and heat shock, and is associated with mitochondrial fragmentation (Al-Mehdi et al., 2012; Agarwal and Ganesh, 2020). This type of positioning is considered adaptive to stresses and cytoprotective. Microtubule polymerization inhibitors, such as nocodazole (NC) and Cholchicine, and the expression of KinAΔN355 mutant of Kinesin prevent it, indicating that microtubule- and Dynein and Kinesin-dependent. Mitochondria may be transported along the microtubule track. PNMC participates in cancer adaptation to hypoxia through mitochondrial ROS production and Hypoxia-inducible factor-1α, the master transcription factor of hypoxic signaling (Al-Mehdi et al., 2012). Recently, we reported that air plasma-activated medium (APAM) exhibits potent anticancer activity against osteosarcoma (OS) and oral cancer (OC) by triggering apoptosis or nonapoptotic cell death (Suzuki-Karasaki et al., 2022). Notably, another type of mitochondrial distribution was associated with this effect. Namely, mitochondria become fragmented and gather one side of the perinuclear sites. Drastic changes in the shape and location of tubulin accompany this movement. Like mitochondria, tubulin concentrates one side of the nuclei. NC and antioxidants prevent these changes, suggesting the involvement of ROS and mitochondrial transport mechanisms similar to PNMC. We named this unique mitochondrial positioning monopolar perinuclear mitochondrial clustering (MPMC) to distinguish it from other known mitochondrial locations.

A recent report demonstrates the production of O_3 in a PTS and the correlation between the amount and antitumor activity (Mokhtari et al., 2019). However, no further evidence is demonstrated for the oxidant's role in the media's action. Another group compared the antitumor activity between different CAPs and gaseous O_3, indicating that the gas had much faster and cytotoxic effects via cyclophilin D-related necrosis (Lunov et al., 2014, 2017). We found that APAM contained significant amounts of O_3 and sought to clarify the involvement of this oxidant in tumor-selective cytotoxicity. For this purpose, we created a NOx-free ozonated medium (ODM) and tested its impact on cancer cell survival. Results showed that this medium could mimic the biological effects, including MPMC, oxidative cell death, and tumor-selective anticancer activity.

2. Materials and methods

2.1. Materials

Unless otherwise specified, all chemicals were obtained from Sigma-Aldrich (St. Louis, MO, USA). The pan-Caspase inhibitor Z-VAD-FMK was obtained from Merck Millipore (Darmstadt, Germany). All insoluble reagent was dissolved in dimethyl sulfoxide (DMSO), and the stock solutions were diluted in 10% Fetal Bovine Serum (FBS) contained Dulbecco's Modified Eagle Medium (DMEM; final DMSO concentration, < 0.1%) before use.

2.2. Cell culture

The human OC cell line HOC313 was kindly provided by the Department of Oral and Maxillofacial Surgery, Graduate School of Medical Science, Kanazawa University (Kanazawa, Japan). Another human OC cell line SAS and glioblastoma (GBM) cell lines, A172 and U251MG were obtained by the Japanese Collection of Research Bioresource (JCRB) Cell Bank of the National Institute of Biomedical Innovation, Health, and Nutrition (Osaka, Japan). Human fetal osteoblasts (hFOB) were a kind gift from Dr T. Ando (Yamanashi University). Human dermal fibroblasts (HDFs) were obtained from Cell Applications (San Diego, CA, USA). The cells were maintained in 10% FBS (Serena Europe GmbH, Brandenburg, Germany) containing DMEM (Merck, NM, USA) supplemented with 100 U/mL penicillin and 100 μg/mL

streptomycin (FBS/DMEM) at 37 °C in a 5% CO_2 incubator.

2.3. O_3 and ODM preparations

O_3 was generated using the O_3 generator (Tokyo Keiki Inc.) equipped with a dielectric barrier discharge probe illustrated in Fig. 1. This generator can produce high concentrations of O_3 from highly pure O_2 (99.9%) (Taiyo Nippon Sanso JFP Corporation, Kanagawa, Japan). It does not allow air contamination and the resulting excitation of N_2. The formed O_3 was introduced into phenol red-free DMEM (Fuji Film Wako Chemicals. Osaka, Japan) by bubbling, producing an ozonated medium (ODM hereafter). The typical experiment conditions are a 10–15 KV voltage and a gas flow rate of 0.4 L/min. ODM was made by O_3 bubbling at the ratio of 1 min bubbling/1 mL medium. The original ODM was diluted to a final concentration of 6.3–50% with phenol red-free DMEM (for biochemical experiments) or FBS/DMEM (for cell experiments).

2.4. APAM preparation

Air plasma and APAM were prepared as reported previously (Suzuki-Karasaki et al., 2022). Briefly, the plasma was generated from the ambient air using a Piezobrush™ PZ2 model plasma jet (relyon Plasma GmbH, Regensburg, Germany) equipped with a piezo element. The APAM (1 mL) was made by flushing the plasma to phenol red-free DMEM for 1 min at a distance of 20 mm. The original APAM was diluted to a final concentration of 6.3–50% with the medium (biochemical experiments) or FBS/DMEM (for cell experiments).

2.5. Quantitation of oxidants

The O_3 concentrations in serially diluted solutions were routinely measured by a Digital Pack Test (DPM2-O_3, range 0.25–5 mg/L, Kyoritsu Chemical-Check Lab. Corp., Kanagawa, Japan). This test minimally cross-reacted with H_2O_2 up to 1 mM. O_3 concentrations were also measured by a polarographic O_3 meter (DOZ-1000PE, Custom Corporation, Tokyo, Japan). According to the manufacturer's protocols, H_2O_2 was quantitated using HYDROP-EX™ (Goryo Chemicals, Sapporo, Japan) according to the manufacturer's. The concentrations of NO_2^- and NO_3^- were measured using a Kit (NO_2 / NO_3 Assay Kit-CII(Colorimetric) Griess Reagent Kit, Dojindo, Kumamoto, Japan) according to the manufacturer's protocols. The H_2O_2, NO_2^-, and NO_3^- concentrations were calculated using a standard curve made using the authentic samples from the kit.

2.6. Cell viability assay

Cell viability was measured by the WST-8 assay using a Cell Count Reagent SF (Nacalai Tesque, Inc, Kyoto, Japan). Cells in FBS/DMEM

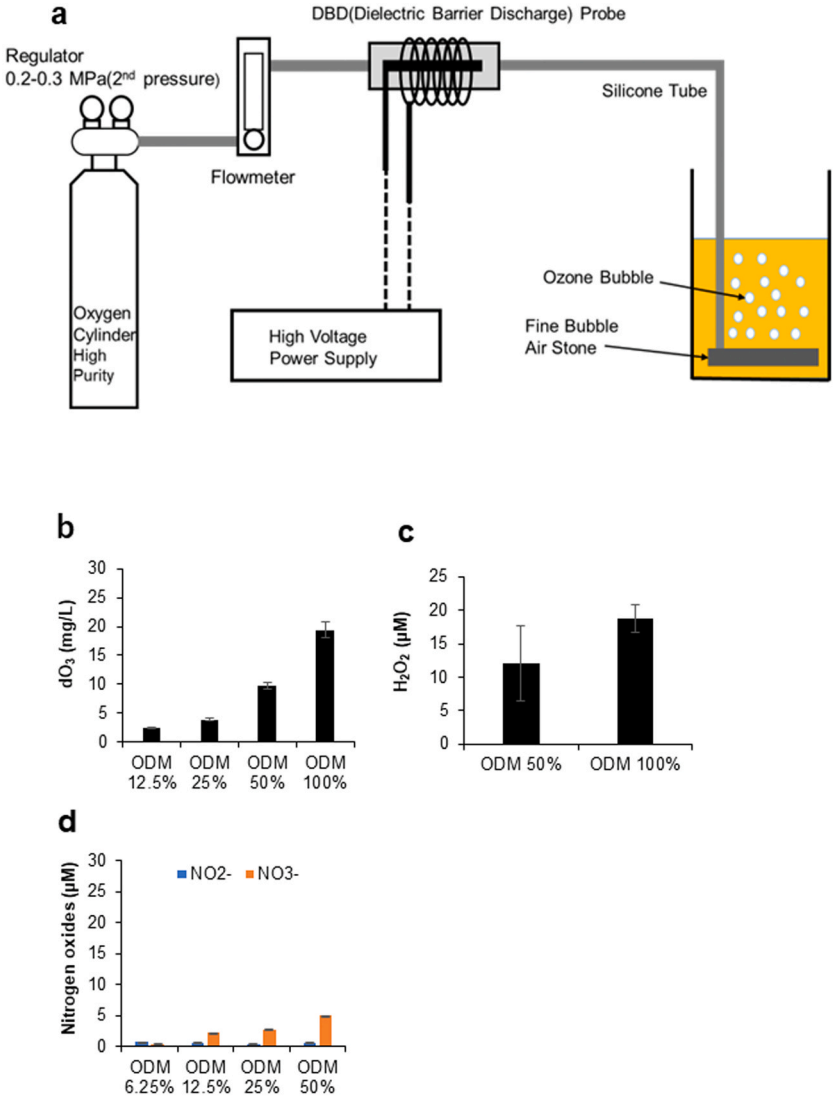

Fig. 1. ODM has O_3 and H_2O_2 but not NO_2^-/NO_3^-. (a) Schematic O_3-generator and bubbling system diagrams. O_3 was generated by exciting high-purity (99.9%) molecular oxygen (O_2) with dielectric barrier discharge. The resulting O_3 was then introduced into a DMEM by bubbling. (b, c) Quantitation of dissolved O_3 (dO_3) and H_2O_2 in ODM. The amounts of O_3 (b) and H_2O_2 (c) in ODM (12.5–100% solution) were measured as described in Materials and Methods. Data are the mean ± SD (n = 4). (e) The concentrations of NO_2^- and NO_3^- in ODM (6.3–50% solution) were measured using the Griess method. NO_3^- concentration was calculated following the formula; $[NO_3^-] = [(NO_2^- + NO_3^-)] - [NO_2^-]$. Data are the mean ± SD (n = 4).

were plated at 4×10^3 cells/well in 96-well plates (Corning Incorporated, NY, USA). They were incubated at 37 °C overnight, added with agents, and incubated for 72 h. In the resistance assay, agents were added after incubating cells for 72 h. This prolonged preincubation allows cells to reach a higher density and become less sensitive to agents. After treatment, cells were added 10 μL of Cell Count Reagent SF and further incubated for 2 h. Absorbances at 450 nm were measured by a Nivo 3 F Multimode Plate Reader (PerkinElmer Japan Company, Ltd., Yokohama, Japan).

2.7. Cell death assay

Whole-cell death was evacuated by fluorescence microscopy as previously described (Suzuki et al., 2012) with minor modifications. Briefly, cells in FBS/DMEM were seeded at 1.5×10^4 cells/well in a 35 mm Poly-Lysine-coated glass bottom dish (D11531H, Matsunami Glass Ind. Corp., Osaka, Japan) and treated with agents at 37 °C overnight in a 5% CO_2 incubator. After removing the medium by aspiration, the cells were stained with 4 μM each of Calcein-AM and Ethidium homodimer-1 (EthD-1) for 30 min to label live and dead cells, respectively, using a kit (LIVE/DEAD Viability/Cytotoxicity kit). Cells were washed and immersed in FluoroBrite™ DMEM. Images were obtained using BZ-X 710 Digital Biological Microscopy (Keyence, Osaka, Japan) with a 40 × , 0.60 numerical aperture (NA) LUCPlanFL N Objective (Olympus Corporation, Tokyo, Japan) and were analyzed by BZ-H3A application software (Keyence).

2.8. Imaging of mitochondria and tubulin

The mitochondrial morphology, positioning, and tubulin dynamics were analyzed as previously described (Suzuki-Karasaki et al., 2022). Briefly, cells FBS/DMEM were seeded at a 5×10^4/mL density in a 35 mm Poly-Lysine-coated glass bottom dish, as described above and treated with agents at 37 °C for 2 or 18 h in a 5% CO_2 incubator. After removing the medium, the cells were stained with 20 nM MitoTracker™ Red CMXRos (MTR) or MitoTracker™ Green FM (MTG, ThermoFisher). The nuclei were counterstained with 1 mg/mL of Hoechst33342 for 1 h at 37 °C in a 5% CO_2 incubator. Tubulin was stained with Tubulin Trackerr™ Green (TTG, ThermoFisher). After washing with FluoroBrite™, the cells were immersed in FluoroBrite™. Images were obtained using a BZ X-710 Digital Biological Microscope (Keyence, Osaka, Japan) equipped with a 100 × , 1.40 n.a. UPlanSApo Super-Apochromat, coverslip-corrected oil objective (Olympus) and analyzed using BZ-H3A application software (Keyence). For each experimental group, the mitochondria in 2 or 3 different pictures were counted for three different distribution patterns, pan-cytoplasmic (Type I), PNMC (Type II), and MPMC (Type III).

2.9. Analyses of ROS and lipid radicals

Cells were seeded in a 35 mm Poly-Lysine-coated glass bottom dish and treated with agents at 37 °C for 2 h in a 5% CO_2 incubator. After removing the medium, the cells were stained with 1 μM OxiORANGE™ (OXO), HYDROP™ (Hydrop, Goryo Chemicals), 5 μM MitoSOX™ Red (MitoSOX, ThermoFisher), and LipiRADICAL Green (LipRG, Funakoshi Corporation, Tokyo, Japan), to detect $^{\bullet}OH$, H_2O_2, $O_2^{\bullet-}$, and lipid peroxyl radicals ($LOO^{\bullet}$), respectively. Images were obtained using BZ-X 710 Digital Biological Microscopy fluorescence microscopy and analyzed using BZ-H3A application software as described above. Luminescence in pictures in about 20 samples for each group was quantitated using the freely available NIH ImageJ software (NIH, Bethesda, MD, USA).

2.10. Analysis of intracellular iron

As described above, cells growing in a 35 mm Poly-Lysine-coated glass bottom dish were treated with agents at 37 °C for 2 h in a 5% CO_2 incubator. Cellular labile iron pools (LIPs), possibly within the Golgi apparatus (GA) and endoplasmic reticulum (ER), are analyzed using the Fe (II)-specific probes FerroOrange (FO) and FeRhoNox™-1 (FeR) (Dojindo Laboratories, Kumamoto, Japan) (Hirayama, n.d.). Mitochondrial LIPs were detected by the organelle-targeted Fe (II)-specific probe Mito-FerroGreen (Dojindo). Images were obtained and analyzed as described above and quantitated as described above.

2.11. Statistical analysis

Data are presented as mean ± standard deviation (SD) and analyzed by a one-way analysis of variance followed by Tuckey's post hoc test using statistical software with Excel 2019 for Windows (SSRI, Tokyo, Japan). $P < 0.05$ was considered statistically significant.

3. Results

3.1. ODM has O_3 and H_2O_2, but not NO_2^- and NO_3^-

Measurements of oxidants revealed that APAM had considerable amounts of O_3, in addition to approximately 30 μM H_2O_2 and 100 μM NO_2^- and NO_3^- (Supplementary Fig. 1a—c). These findings led us to explore the possible role of O_3 in the biological effect of APAM. For this purpose, we produced an ozonated medium (ODM) using the system illustrated in Fig. 1a. This medium contained O_3 at dozens μM (Fig. 1b). The amount was increased over introducing time for at least 30 min. ODM also had approximately 20 μM H_2O_2 but NO_2^- and NO_3^- were under detection limits (Fig. 1c, d).

3.2. ODM can kill different cancer cells

Next, we examined whether ODM affected cancer cell survival. Cells were treated with varying concentrations (12.5–50% solution) of ODM for 72 h and analyzed for cell viability. The treatment dose-dependently decreased the viability of OC cell lines, such as SAS and HOC-313 (Fig. 2a, b). ODM had similar effects in several OS and GBM cell lines, including HOS and U251MG (Fig. 2c, d). Cellular sensitivity to ODM varied considerably depending on the cell line and density. In high-responding cells, ODM (≤12.5%) was enough to reduce viability potently (≥50% reduction), while in low-responding cells, higher doses (≥25%) were required for a moderate effect (around 50% reduction). Robust cell and nuclear morphological changes accompanied the impact. Most untreated cells were adherent spindle cells with smooth surface round nuclei. Meanwhile, ODM-treated cells exhibited blebbing, rounded shapes, most of which lost membrane integrity and had shrunk and deformed nuclei (Fig. 2e, f). These results show that ODM can injure different cancer cell types. In the following experiments, we analyzed the effect of ODM in detail using OC cells as a model.

3.3. ODM primarily induces oxidative cell death in an H_2O_2-dependent manner

To understand the mechanism underlying cell injury, we examined the effect of cell death inhibitors . Z-VAD-FMK and Necrostatin-1 (Nec-1) minimally prevented the cytotoxic effect in SAS and HOC-313 (Fig. 3a, b). Chloroquine (CQ) and 3-Methyladenine (3-MA) were ineffective, either (not shown). Instead, the H_2O_2-degrading enzyme Catalase abolished the impact in both cells (Fig. 3c, d). In contrast, the superoxide scavenger MnTBaP had no such effect, indicating the specific role of H_2O_2. We also found that Catalase prevented cell death caused by APAM in SAS cells (Supplementary Fig. S1d). These results indicate that, like APAM, ODM primarily induces oxidative cell death in an H_2O_2-dependent manner.

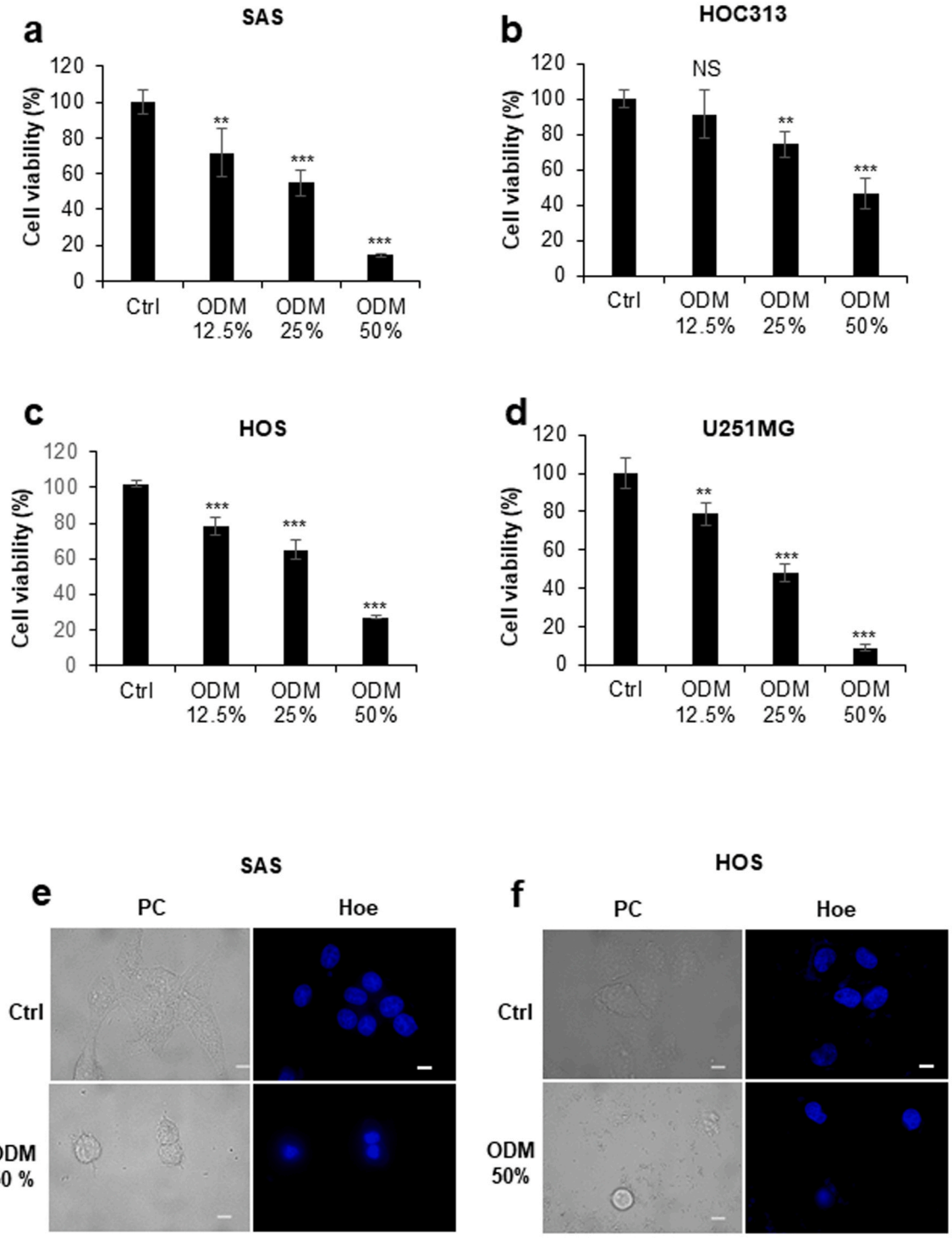

Fig. 2. ODM can injure different cancer cell lines. (a—d) SAS (a), HOC-313 (b), HOS (c), and U251MG (d) cells in FBS/DMEM were plated at 4×10^3 cells/well and incubated overnight. The cells were treated with ODM (12.5–50% solution) for 72 h and analyzed for growth using a WST-8 cell growth assay. Data are the mean ± SD (n = 8). Data were analyzed by one-way analysis of variance followed by Tukey's post hoc test. * $*P < 0.01$; * $**P < 0.001$; NS, not significant vs. control treated with vehicle. (e, f) SAS (e) and HOS (f) cells (1.5×10^4 cells/well) were plated in a 35 mm glass bottom dish and incubated overnight, and then treated with ODM (50%) for 2 h. After removing the medium by aspiration, the cells were stained with Hoechst33342 (Hoe). Images were obtained from BZ-X 710 Digital Biological Microscope equipped with a 100x objective and analyzed using BZ-H3A application software. PC, phase contrast. Scale bar = 10 μm.

3.4. ODM increases mitochondrial ROS in an H_2O_2- and iron-dependent manner

As APAM increases intracellular ROS, including those within mitochondria (Suzuki-Karasaki et al., 2022), we examined whether ODM also could affect cellular ROS levels. Analysis using the oxidant-specific probe MitoSOX revealed a significant increase in $O_2^{\bullet-}$ within the mitochondria (Fig. 4a). This increase was observed with substantial cellular and nuclear morphological changes. Moreover, Catalase abolished the effect, indicating its H_2O_2-dependence. Treatment with the irreversible

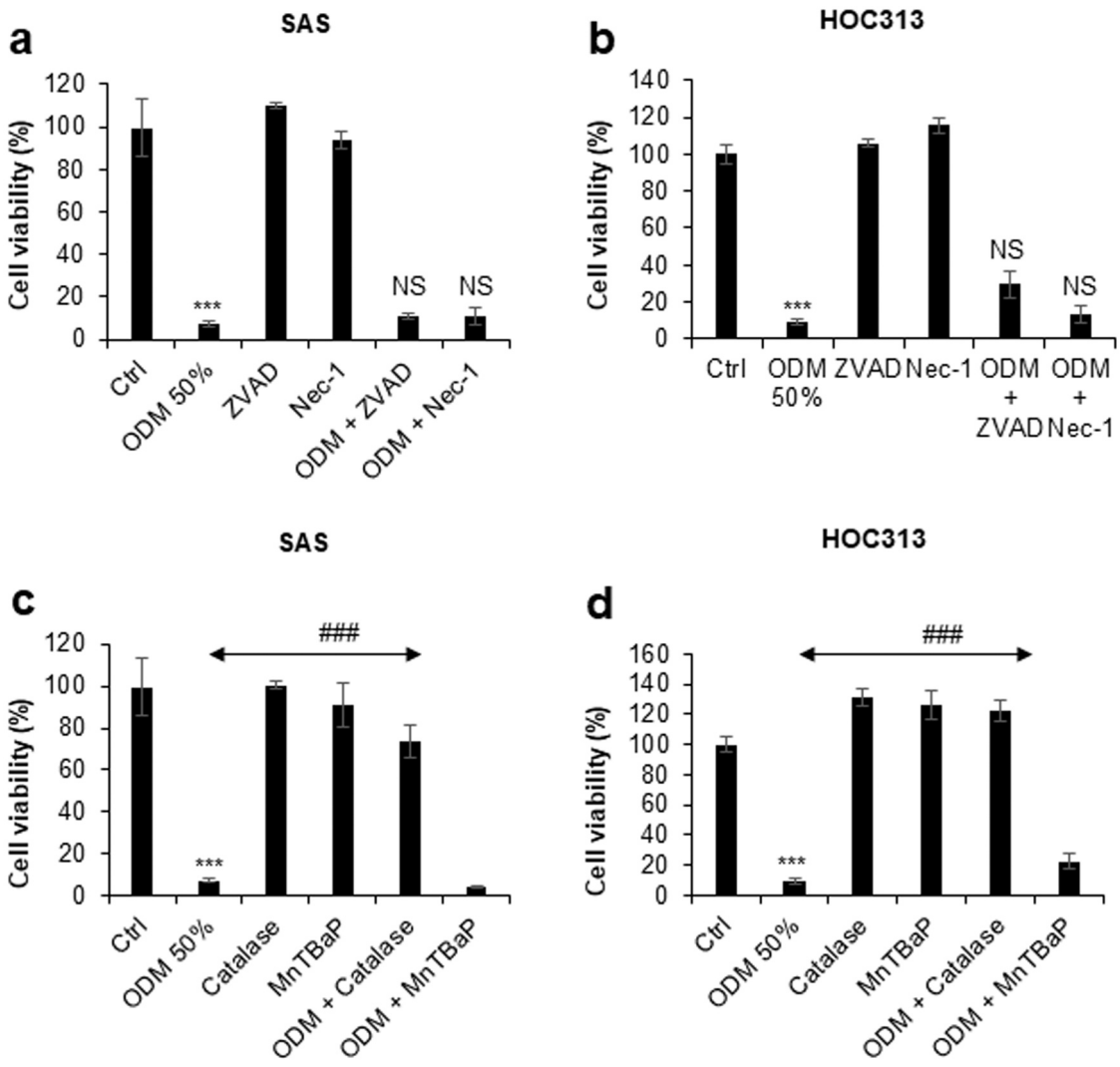

Fig. 3. ODM induces oxidative cell death in an H_2O_2-dependent manner. (a, b) Effect of cell death inhibitors on ODM cytotoxicity. SAS (a) and HOC-313 (b) cells were processed as described in the legend of Fig. 2. The cells were incubated with 10 μM Z-VAD-FMK, 1 μM Ferrostain-1 (Fer-1), or 30 μM Necrostatin-1 (Nec-1) for 1 h and then treated with ODM (50%) for 72 h. The cell growth was measured as described in the legend of Fig. 2. Data are the mean ± SD (n = 8). Data were analyzed by one-way analysis of variance followed by Tukey's post hoc test. * **P < 0.001 vs. control treated with vehicle. ### P < 0.001. NS, not significant vs. control treated with vehicle. (c, d) SAS (c) and HOC-313 (d) cells were incubated with 10 U/mL Catalase or 30 μM MnTBaP for 1 h and then treated with ODM (50%) for 72 h. Data were analyzed by one-way analysis of variance followed by Tukey's post hoc test. * **P < 0.001 vs. control treated with vehicle. ### P < 0.001.

Catalase inhibitor 3-AT increased $O_2^{\bullet-}$(Fig. 4a), further supporting the role of H_2O_2. Fig. 4b shows the quantitative analysis of the increase and supports the results. In addition, the treatment increased $^{\bullet}OH$ detected by OXO, and Catalase also suppressed this effect (Fig. 4c, d). Moreover, ODM increased $LOO^{\bullet}$, detected by LipRG (Fig. 4e). MitoSOX and OXO can detect $O_2^{\bullet-}$and $^{\bullet}OH$ within mitochondria, suggesting increases in mitochondrial ROS (mROS). To test this view, we analyzed the cellular location of the OXO signal. In untreated cells, the signal has broadly distributed the cytoplasm. After ODM treatment, the signal was observed at one side of the perinuclear sites. As a result, it colocalized with mitochondria, and Catalase abolished this shift and the cellular morphological changes (Supplementary Fig. S2a). The basal intracellular $LOO^{\bullet}$ levels varied considerably depending on cell growth conditions. In some cases, OC cells had substantial levels of $LOO^{\bullet}$, and iron (II) chelation by 2,2′-Bipyridyl (BP) significantly reduced them, indicating the involvement of iron in the production (Supplementary Fig. S2b). The primary $LOO^{\bullet}$ were minimally colocalized with mitochondria. In contrast, they were entirely observed in mitochondria around shrunk nuclei after ODM treatment. Iron chelation and Catalase prevented this shift and nuclear damage, suggesting the role of H_2O_2 and iron. These results indicate that ODM increases mROS in an H_2O_2- and iron-dependent manner.

3.5. *Increased H_2O_2 scavenging activity contributes to tolerance to ODM*

We noticed that the effect of ODM decreased as the cell plating density increased. As a result, HOC-313 cells grown at a density of 4-fold higher than the standard conditions became highly resistant to treatment with ODM (50%) (Fig. 5a). As the above results suggested that H_2O_2 was critical in oxidative cell death, we assumed the resistance might result from decreased H_2O_2-scavenging activity. To test this, we examined the impact of agents affecting the activity on ODM cytotoxicity. The glutathione (GSH) synthase inhibitor BSO has been shown to reduce GSH synthesis and GSH-dependent antioxidant systems, including GSH peroxidase (GPX), the primary H_2O_2-scavenging enzyme (Meister, 1995; Jiang et al., 2018). BSO had moderate cytotoxicity and markedly augmented cell death caused by ODM (Fig. 5a, b). BSO also synergistically increased intracellular H_2O_2 with ODM (Fig. 5c). 3-AT can block H_2O_2 removal by Catalase. 3-AT had a similar effect to a lesser extent. Unlike BSO, it alone was minimally cytotoxic but

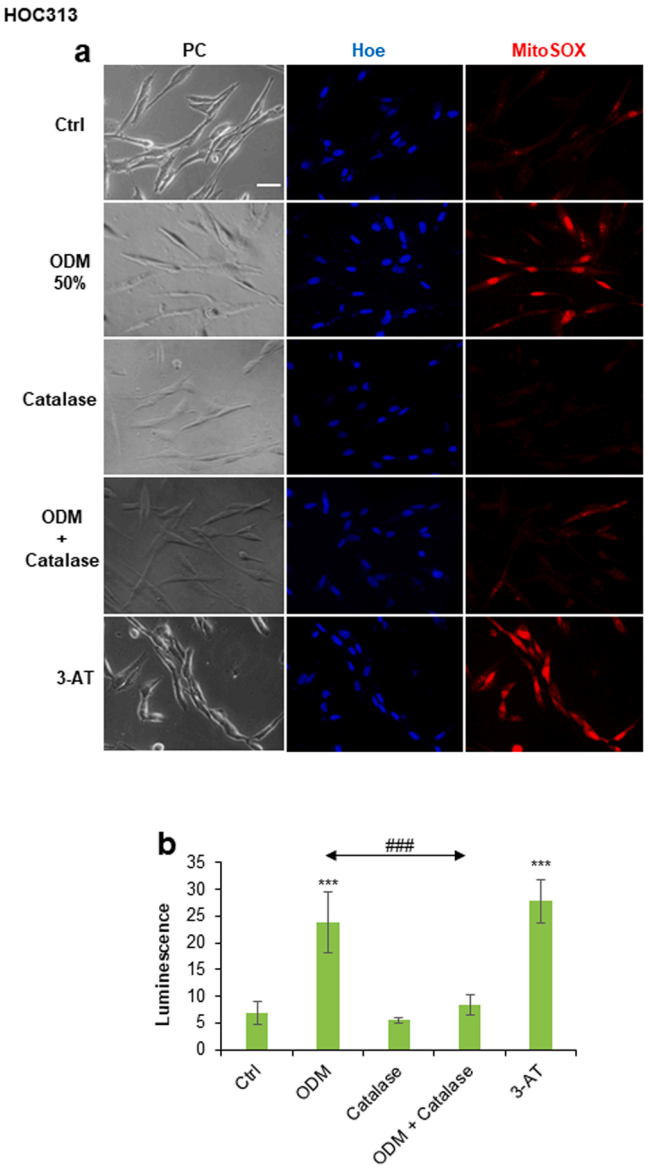

Fig. 4. ODM increases different intracellular ROS in an H_2O_2-dependent manner. (a) HOC-313 cells were preincubated with 3-amino-1,2,4-triazole (3-AT, 1 mM) and Catalase for 1 h and then treated with ODM (50%) for 2 h. Mitochondrial $O_2^{\bullet-}$ and nuclei were stained using specific probes MitoSOX and Hoechst33342, respectively. All images were obtained from BZ-X 710 Digital Biological Microscope with a uniform exposure time). (b) The luminescence of all color images was measured using a NIH ImageJ software. Data are the mean ± SD (n = 9). Data were analyzed by own-way analysis of variance followed by Tuckey's post hoc test. * ** $P < 0.001$ vs. control (Ctrl). ###$P < 0.001$. (c) The cells were pretreated with Catalase for 1 h and then incubated with ODM for 2 h. Intracellular $^{\bullet}OH$ were stained with OXO. The nuclei were counterstained with Hoechst33342. Scale bar = 300 μm. (d) The luminescence of all color images was analyzed as described above. Data are the mean ± SD (n = 8). Data were analyzed by own-way analysis of variance followed by Tuckey's post hoc test.* ** $P < 0.001$ vs. control. ###$P < 0.001$. (e) HOC-313 cells were pretreated with Catalase for 1 h and then incubated with ODM for 2 h. Mitochondria, intracellular $^{\bullet}OH$, $LOO^{\bullet}$, and nuclei were stained with MTG, OXO, LipiRG, and Hoechst33342, respectively. Scale bar = 20 μm.

significantly enhanced cell death (Fig. 5a). These results provide further evidence for the critical role of H_2O_2 in regulating ODM cytotoxicity.

3.6. ODM induces tubulin remodeling and MPMC in an H_2O_2-dependent manner

Aberrant mitochondrial morphological and positioning changes (MPMC) proceed to cell death caused by APAM (Suzuki-Karasaki et al., 2022). Therefore, we examined whether ODM had similar effects. In untreated HOC-313, most mitochondria have Type I (Pan-cytoplasmic) or II (PNMC) distribution. Following ODM treatment, most mitochondria became fragmented and assembled at one side of the damaged nuclei, indicating their phenotype changes into type III (MPMC) (Fig. 6a). These morphological changes occurred as rapidly as within 2 h after ODM treatment. Like ODM cytotoxicity, Catalase prevented the effect. Quantitative analyses of Type I, II, and III mitochondria ratios confirmed these observations (Fig. 6b). Similar impacts were observed in SAS, HOS, and U251MG (Supplementary Fig. S3a–c). The distribution changes suggested the onset of mitochondrial movement. Since mitochondria can move along the microtubule track, we analyzed the impact of ODM on Tubulin dynamics. In untreated cells, Tubulin had a network structure distributing broadly on both sides of the nuclei in the cytoplasm (Pan-cytoplasmic distribution) (Fig. 6c). On the other hand, after ODM treatment, it condensed and assembled around the nuclei in the same direction as mitochondria (Perinuclear distribution). Catalase also prevented the effect (Fig. 6c). Quantitative analyses of the two types of

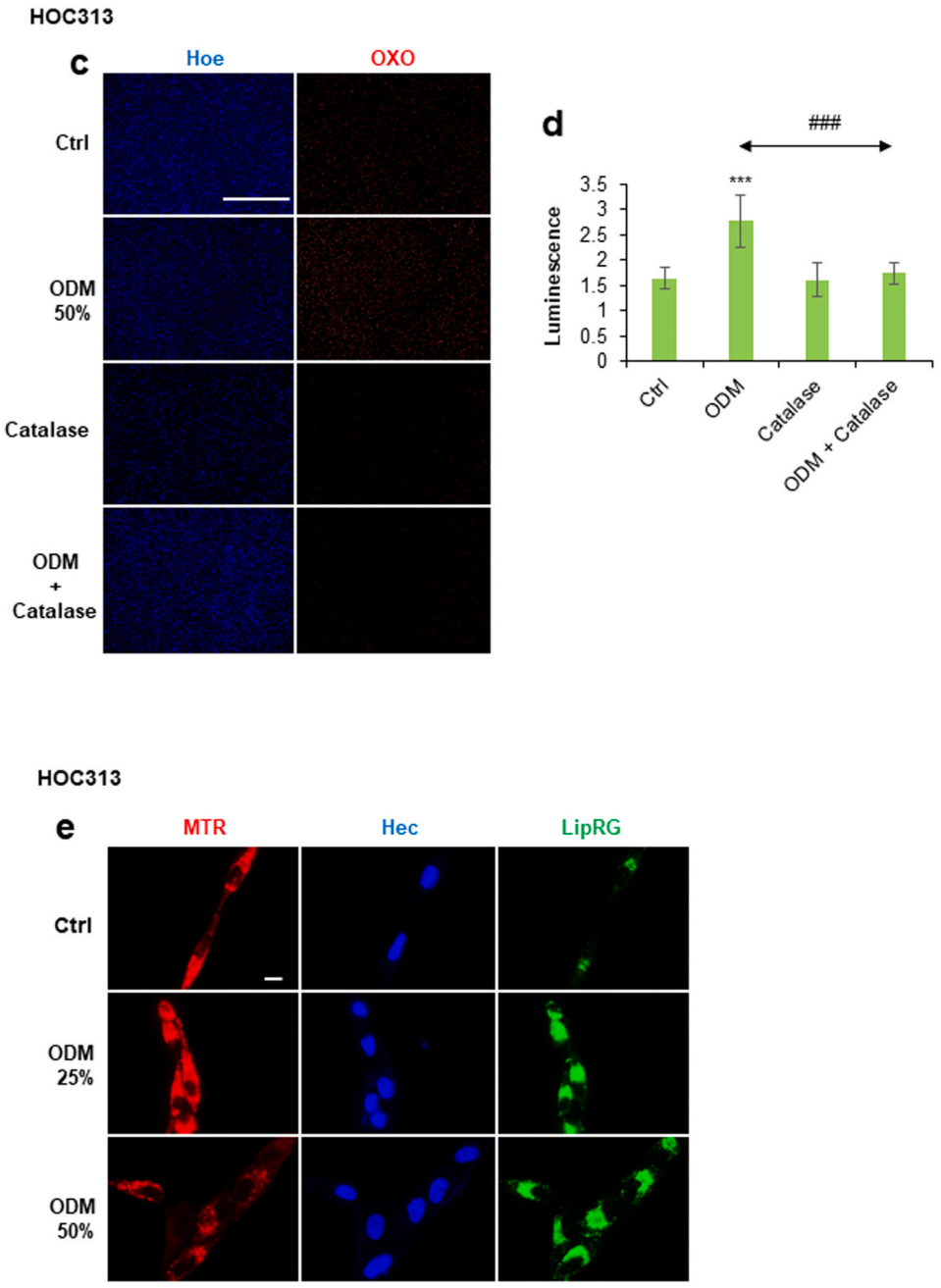

Fig. 4. (*continued*).

Tubulin positioning confirmed these observations (Fig. 6d). Similarly, the microtubule inhibitor NC prevented MPMC and the Tubulin remodeling (Supplementary Fig. S3d). These results indicate that ODM induces MPMC and microtubule remodeling in an H_2O_2-dependent manner.

3.7. H_2O_2 cannot mimic the effects of ODM

ODM contains a substantial amount of H_2O_2 (Supplementary Fig. S1), and this oxidant has been considered a critical mediator of the effects of PTSs. Accordingly, the oxidant could be vital in mediating the effects of ODM. To test this possibility, we examined its ability to affect cell survival. Thirty μM H_2O_2 , which were 2-fold higher than the oxidant in ODM 50%, minimally reduced cell viability in HOC313, TSU, HOS, and 143B cells (Fig. 7a—d). In addition, the oxidant alone failed to induce MPMC in 143B and A172 cells (Fig. 7e, f). These results indicate that H_2O_2 cannot mimic the effects of ODM

3.8. Iron mediates oxidative cell death

Next, we examined whether iron played a role in ODM cytotoxicity. Both BP and DFO reduced the effect of ODM (50%) moderately (around 50% inhibition) under conditions where iron chelation caused modest cytotoxicity (Fig. 8a). In contrast, the ferroptosis inhibitor Ferrostatin-1 (Fer-1) failed to protect cells from ODM cytotoxicity. To gain insight into the possible iron source, we analyzed the cellular LIPs using FeR. This probe can detect iron (II) in the cytoplasm, Golgi apparatus (GA), and endoplasmic reticulum (ER) (Hirayama, n.d.). The signal was significantly decreased after ODM treatment (Fig. 8b, c). At the same time, it was reduced by BP while increased by iron (II) addition. On the other

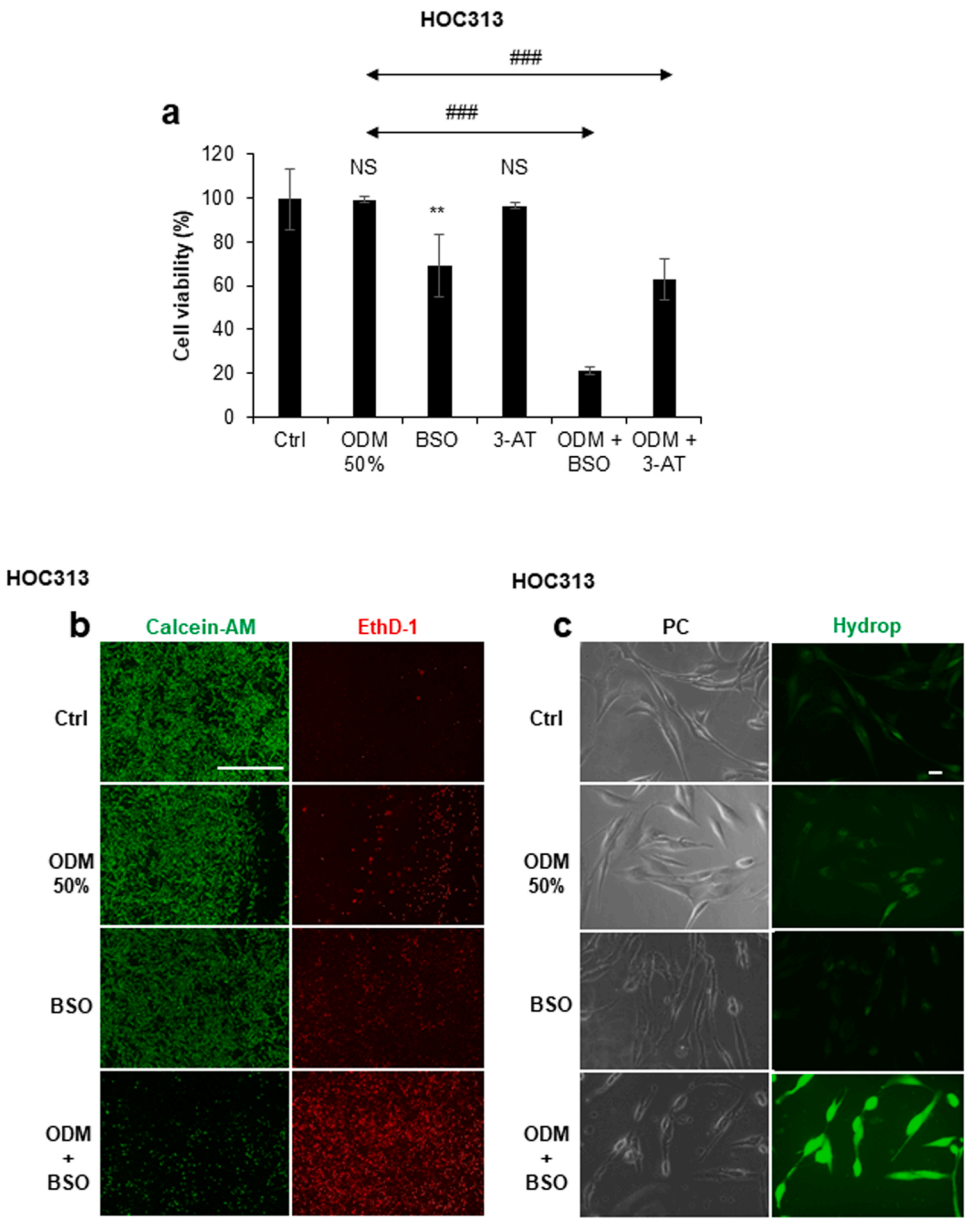

Fig. 5. BSO augments ODM-induced H_2O_2 increase and cell death in insensitive cells. (a) HOC-313 cells were pretreated with the DL-Buthionine-(S, R)-sulfoximine (BSO, 100 μM) or 3-AT (1 mM) alone or in combination for 1 h. then they were treated with the ODM (50%) for 72 h. Cells were analyzed for viability as described in the legend of Fig. 3. Data were analyzed by own-way analysis of variance followed by Tuckey's post hoc test. Data are the mean ± SD (n = 7 or 8). * * $P < 0.01$; NS, not significant vs. control; ###$P < 0.001$. (b) The cells were pretreated with BSO for 1 h and then treated with ODM (50%). They were incubated for 18 h and analyzed for cell death using Calcein-AM (Calcein, 2 μM) and Ethidium homodimer-1 (EthD-1, 2 μM). Live cells were stained green with Calcein, whereas dead/dying cells were stained red with EthD-1. Images were obtained from BZ-X 710 Digital Biological Microscope with a 4x objective. Scale bar = 300 μm. (c) The cells were treated with the ODM (50%) or BSO alone or in combination for 18 h and were stained with HYDROP™ (Hydrop,1 μM). Images were obtained from BZ-X 710 Digital Biological Microscope with a 40x objective and analyzed as previously described in the legend of Fig. 4. Scale bar = 20 μm.

hand, like iron (II) addition, the signal of MTFG, a mitochondria-targeted iron (II) probe (Hirayama et al., 2018), was increased (Fig. 8b, c). Microscopic analysis with a higher resolution validated the colocalization of the MTFG signal and mitochondria (Supplementary Fig. S4). Accordingly, most MTFG signal was distributed broadly in the cytoplasm in untreated cells. According to MPMC, the MTFG signal was gathered at the perinuclear regions of smaller nuclei, and BP mitigated the shift. In addition, BP and DFO also prevented APAM cytotoxicity, while Fer-1 was ineffective (not shown). These results indicate that iron mediates oxidative cell death caused by ODM as well as APAM.

3.9. ODM had low cytotoxicity in nonmalignant cells

Next, we examined whether ODM had cytotoxicity in nonmalignant cells. ODM (≤25%) had minimal effect on the viability of HaCaT and hFOB, the nonmalignant counterparts of OC and OS, respectively (Fig. 9a, b). Only at the highest concentration (50%) ODM decreased cell viability moderately . Moreover, minimal cellular and nuclear morphological changes were observed after ODM treatment in HaCaT and HDFs (Fig. 9c, d). ODM had a minimal effect on mitochondrial morphology in HaCaT while increasing mitochondrial fragmentation but evoked MPMC minimally in HDFs (Fig. 9e, f). In addition, ODM minimally increased intracellular H_2O_2 and mitochondrial $^{\bullet}OH$ in HaCaT (Supplementary Fig. S5). These results indicate that ODM causes minimal MPMC, ROS production, and cell death in nonmalignant cells.

4. Discussion

The present study aimed to examine the antitumor activity of O_3 in solutions and verify its role in mediating the action of APAM. As expected, ODM had considerable amounts of O_3 (Fig. 1) and potent cytotoxicity in various cancer cells, including OC, OS, and GBM (Fig. 2). Moreover, it primarily triggered oxidative cell death in OC cells (Fig. 3). Catalase but not MnTBaP prevented ODM cytotoxicity, suggesting the specific role of H_2O_2. In support of the vital role of H_2O_2-mediated oxidative stress, ODM increased mitochondrial ROS, such as $O_2^{\bullet-}$ and $^{\bullet}OH$, in an H_2O_2-dependent manner (Fig. 4). Conversely, reduced H_2O_2-removal upregulated the oxidant production (Figs. 4 and 5). These results are similar to those obtained with APAM previously described

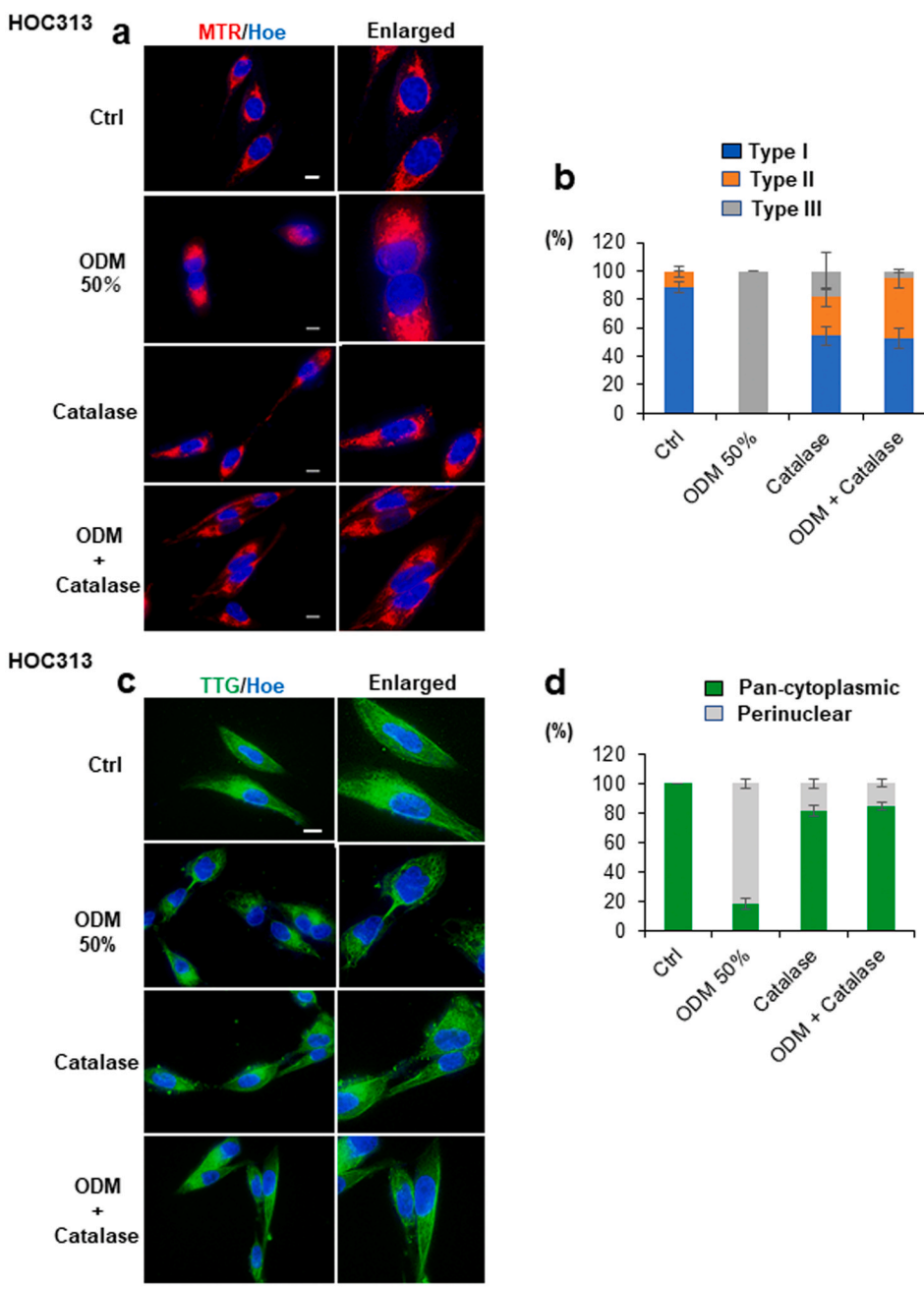

Fig. 6. ODM induces MPMC and Tubulin remodeling in an H_2O_2-dependent manner. (a) After treating HOC-313 cells with medium or ODM (50%) for 2 h, mitochondria and nuclei were stained with 20 nM MTR and Hoechest33342, respectively. Images were obtained from BZ-X 710 Digital Biological Microscope with a 100x objective and analyzed using BZ-H3A application software. Bar = 10 μm. (b) Mitochondria exhibiting three different subcellular distributions, Pan-cytoplasmic (Type I), PNMC (Type II), and MPMC (Type III), were counted in two or three pictures. Data are the mean ± SD (n = ~20). (c) The cells were treated with ODM (50%) for 2 h and stained with Tubulin Tracker™ Green (TTG, 100 nM) for 30 min. Scale bar = 10 μm. (d) Cells with Tubulin exhibiting Pan-cytoplasmic or Perinuclear distribution were counted in two or three pictures. Data are the mean ± SD (n = ~20).

(Suzuki-Karasaki et al., 2022). Moreover, APAM had O_3 as much as ODM (Supplementary Fig. S1). APAM has potent antitumor activity against different cancer cell lines. More importantly, it exhibits tumor--selectivity(Suzuki-Karasaki et al., 2022). Notably, the present data indicate that ODM has a similar effect. ODM showed little cytotoxicity against nonmalignant cells and minimally increased MPMC and ROS production (Fig. 9). ODM had NO_2^- and NO_3^- below the detection limits (Fig. 1), indicating that the effect is NOx-independent.

It is known that O_3 in solutions can generate H_2O_2 in the reaction with H_2O. Our previous study demonstrated that H_2O_2 increased mitochondrial $O_2^{\bullet-}$ by reducing the electron transport chain in different cancer cells (Inoue and Suzuki, 2013). In addition, H_2O_2 also can generate $^{\bullet}OH$ in reacting with $O_2^{\bullet-}$ or transient metal ions such as Iron (II) and Copper (I). Collectively, H_2O_2 produced from O_3 could trigger mitochondrial oxidative stress. In line with this, we observed substantial H_2O_2 in ODM (Fig. 1). Another finding that GSH synthesis inhibition sensitized tolerant cells to ODM (Fig. 5) supports this view. These observations suggest that the GSH-dependent H_2O_2-removal mechanism, possibly GPXs, is vital in removing H_2O_2 after ODM treatment. The inhibition of catalase activity by 3-AT increased mitochondrial ROS but minimally affected cell survival (Figs. 4 and 5). suggesting that in addition to H_2O_2, another event is required to cause cell death in tolerant cells. Notably, like APAM, ODM exhibits tumor-selectivity. It is widely accepted that the antioxidant systems are inactivated in cancer cells due to their high requirement of oxidants in the growth signals. Therefore, decreased H_2O_2-scavenging activity in cancer cells could make them susceptible to ODM cytotoxicity. In contrast, nonmalignant cells have H_2O_2-scavenging activity enough to abolish this oxidant, similar to ODM-tolerant cancer cells. As a result, ODM may exhibit cytotoxic effects more pronouncedly in cancer cells than in nonmalignant cells.

We found that H_2O_2 up to 30 μM (2-fold higher than that in ODM

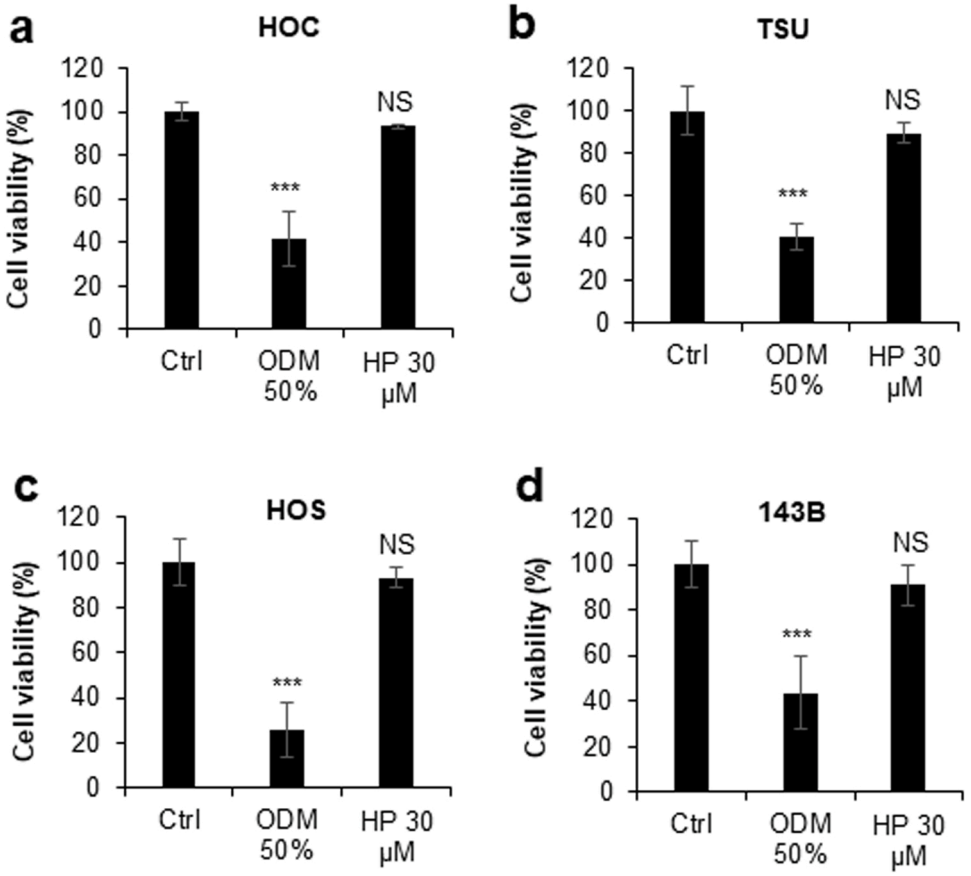

Fig. 7. H_2O_2 cannot mimic the effects of ODM. (a-e) HOC-313 (a), TSU (b), HOS (c), and 143B (d) cells were treated with ODM (50%) or 30 μM H_2O_2 (HP) for 72 h and were measured for viability by a WST-8 assay. Data were analyzed by own-way analysis of variance followed by Tuckey's post hoc test. * **P < 0.001 vs. control treated with vehicle. NS, not significant vs. control treated with vehicle. (e, f) After treating 143B (e) and A172 cells (f) cells with ODM (50%) or 30, 100 μM H_2O_2 (HP) for 2h, mitochondria and nuclei were stained with MTR and Hoechest33342, respectively. Images were obtained from BZ-X 710 Digital Biological Microscope with a 100x objective and analyzed using BZ-H3A application software. Bar = 10 μm.

50%) did not induce MPMC nor decrease cell viability in different cancers (Fig. 7). These findings are consistent with the above observations that H_2O_2 is insufficient for triggering cell death. Removing Iron by specific chelators prevented ODM cytotoxicity (Fig. 8), indicating the vital role of Iron. In line with this, ODM modulated the intracellular iron dynamics; It decreased the FeR signal while increasing the MTFG signal (Fig. 8). FeR can primarily detect Iron (II) within GA and/or ER, while MTFG can react with Iron (II) within mitochondria specifically (Hirayama et al., 2018; Hirayama, n.d.). Accordingly, our data indicate decreased Iron (II) in GA and/or ER and increased mitochondrial Iron (II). It is unclear whether these changes are directly linked, but this finding raises the possibility that ODM might induce Iron transport from GA and/or ER to mitochondria. Further investigations are necessary to solve this problem. Ferroptosis has emerged as a critical oxidative cell death form in cancer cells. It is regulated necrosis resulting from LPO accumulation where GPX and Iron are crucial (Dixon and Stockwell, 2014; Hassannia et al., 2019; Stockwell, 2022). ODM could increase $^{\bullet}OH$ and $LOO^{\bullet}$, the initiators of lipid peroxidation (Fig. 4), consistent with the role of Iron. Accordingly, $^{\bullet}OH$ generation from H_2O_2 and Iron (II) via the Fenton reaction might contribute to oxidative stress via lipid radical production. This view favors the notion that in addition to H_2O_2, other factors are essential for sufficient cell death. However, our data indicate differences from ferroptosis. The failure of Fer-1 in protecting cells from ODM (Fig. 3) suggests the role of different mechanisms and radicals. It is interesting whether APAM also triggers similar cell death mechanisms. Indeed, APAM could induce H_2O_2-dependent oxidative cell death (Supplementary Fig. S1). On the other hand, Iron removal had varying effects on cell death, depending on the cell line and the growing states. Further characterization, including the role of several master ferroptosis regulators and genes in ODM and APAM-induced cell death, is underway.

MPMC may involve three steps: mitochondrial fission, movement, and assembly. The delicate balance between fission and fusion of the mitochondrial membrane regulates the dynamics and macroscopic morphology. Dynamin-related proteins (Drps) with GTPase activity, such as Drp1, Optic atrophy 1 (OPA1), and Mitofusin 1/2 (Mfn1/2), regulate the dynamics concertedly. Drp1 regulates fission, while OPA1 and Mfn1/2 control fusion and cristae organization. Consequently, a defect in either process causes severe mitochondrial and cellular dysfunctions (Twig and Shirihai, 2011; Hoppins and Nunnari, 2012). As mitochondrial fission facilitates eliminating damaged mitochondria through mitophagy-mediated disruption, its deficiency leads to a hyperfused mitochondrial network and compromised mitochondrial quality control. On the other hand, as mitochondrial fusion facilitates the exchange of mitochondrial DNA and metabolites required for mitochondrial function, its failure leads to mitochondrial fragmentation, reduced mitochondrial DNA, growth, mitochondrial membrane potential, and defective respiration. Phosphorylation is the primary regulatory mechanism for Drp1 activity. Phosphorylation of Drp1 at Ser 616 residue promotes Drp1 activation and association with Fission protein 1 (Fis1), leading to the activation of mitochondrial fission. Conversely, Drp1 phosphorylation at Ser 627 residue promotes its inhibition. Previously, we have reported that H_2O_2 increases mitochondrial $O_2^{\bullet-}$ in cancer cells and biases Drp1 phosphorylation toward Ser 616

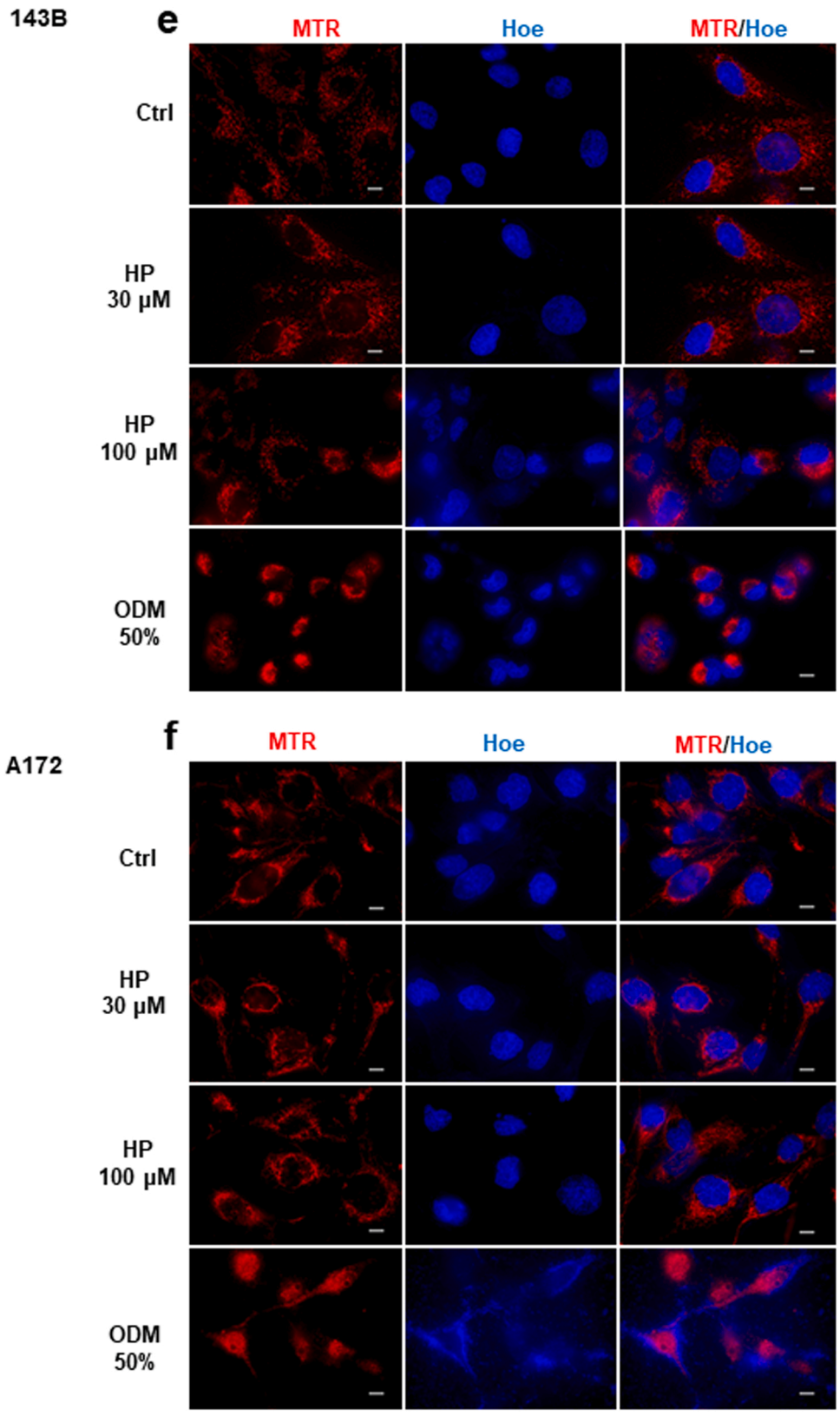

Fig. 7. (*continued*).

predominately, leading to mitochondrial fragmentation (Saito et al., 2016). Antioxidants can prevent MPMC, suggesting the involvement of a similar oxidative pathway in mitochondrial fragmentation during MPMC. In support of this notion, increased $O_2^{\bullet-}$ within mitochondria proceeds to MPMC caused by APAM (Suzuki-Karasaki et al., 2022). Our results showed that ODM also could cause MPMC and Tubulin remodeling (Fig. 6). Notably, Catalase blocked these two events, indicating the critical role of H_2O_2 in regulating MPMC and Tubulin remodeling. Tubulin polymerization is essential in altered mitochondrial distribution from Type I to Type II in response to stresses, such as hypoxia and heat

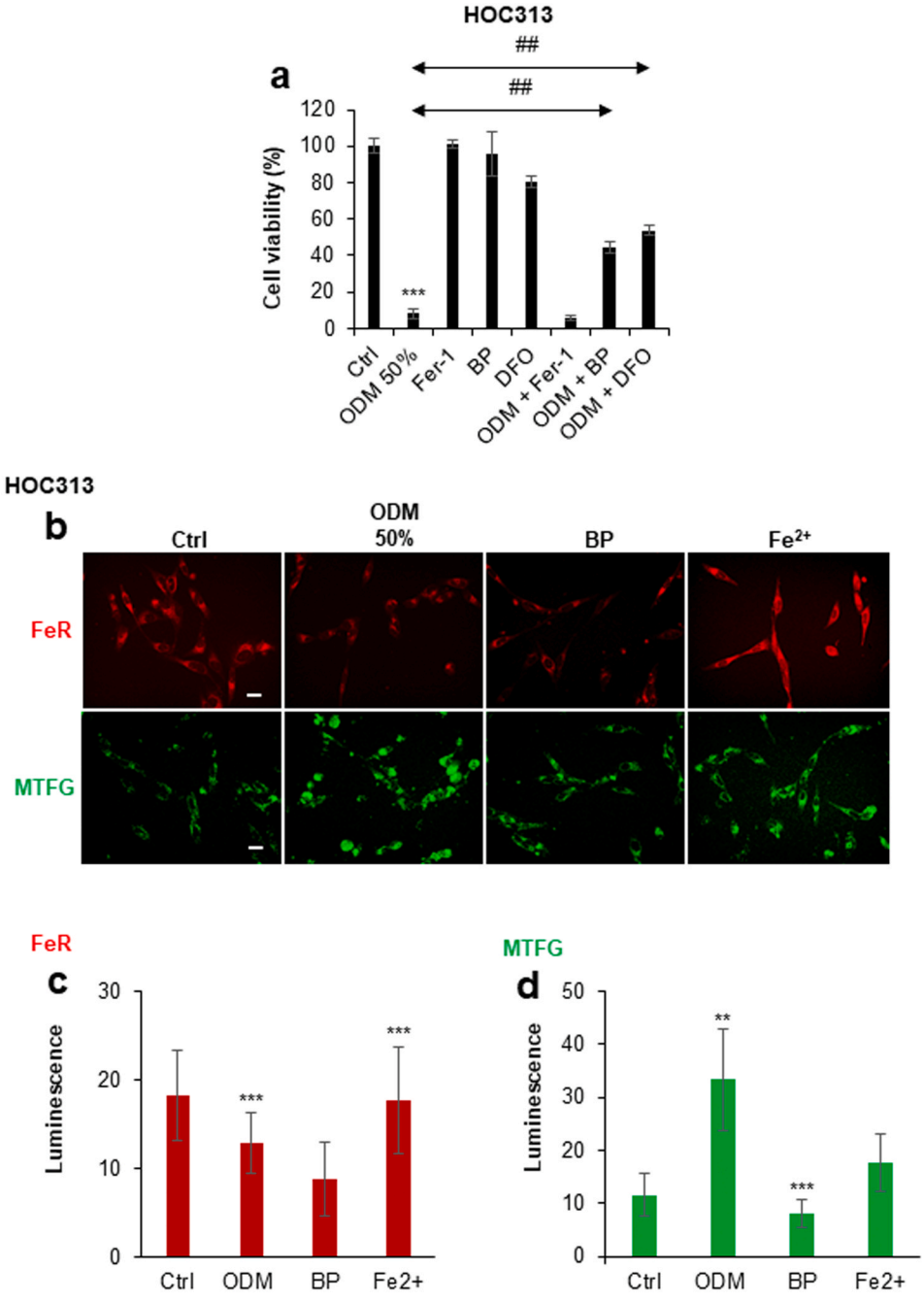

Fig. 8. ODM induces cell death in an iron-dependent manner. (a) HOC-313 cells were pretreated with 100 μM each of 2,2′-bipyridyl (BP), deferoxamine (DFO), or Ferrostatin-1 (Fer-1, 1 μM) alone or in combination for 1 h. Then they were treated with the ODM (50%) for 72 h. Cells were analyzed for viability as described in the legend of Fig. 3. (b) The cells were treated with the ODM (50%) for 2 h and were stained with FeRhoNOX-1 (FeR) or Mito-Ferro Green (MTFG). Images were obtained from BZ-X 710 Digital Biological Microscope with a 40x objective and analyzed as previously described in the legend of Fig. 4. Scale bar = 20 μm. (c, d) The luminescence of FeR and MTFG images was analyzed as described above. Data are the mean ± SD (n = 15–22).

shock (Al-Mehdi et al., 2012; Agarwal and Ganesh, 2020). This event is required for the mitochondrial movement along the microtubule track by motor proteins such as Kinesin and Dynein. Our data indicate that Catalase (Fig. 6) and NC (Supplementary Fig. S2) can prevent Tubulin remodeling and MPMC caused by ODM, suggesting the involvement of H_2O_2 and Tubulin polymerization in the mitochondrial movement. In addition to mitochondrial oxidative stress, plasma membrane depolarization (PMD) is essential for mitochondrial assembly (Suzuki-Karasaki et al., 2015). Notably, O_3 in solutions can affect biological systems in several different forms. It can react with target biomaterials directly and specifically as O_3 itself. It can also attack poly unsatisfied fatty acids (PUFAs) in the cell membrane, resulting in lipid oxides. The production follows PUFA peroxidation and the production of other toxic radicals and substances, such as lipid oxides, lipid peroxides, lipohydroperoxides, 4-Hydroxy-2,3 trans-noneal, and Malonyl dialdehyde (Clavo et al., 2018). These radicals and aldehydes are toxic and could contribute to ODM cytotoxicity. Linoleic acid hydroperoxide can depolarize plasma membrane and mitochondrial membrane potentials (Forman and Kim, 1989). Therefore, LPOs like lipid hydroperoxides might trigger PMD and mitochondrial assembly. Further studies are needed to validate this scenario.

Several prior studies have implicated the role of O_3 in the antitumor effect of PTSs. Mokhtari and colleagues (2009) have shown the production of O_3 in plasma-activated media and the correlation between the amount and antitumor activity. However, this report lacks further evidence for the oxidant's role in the media's action. Lunov et al., (2014, 2017) have demonstrated that O_3 is an abundant component of air plasma and that O_3 gas flush induces necrosis. There are some discrepancies between our results and theirs. The authors reported the highest toxicity of O_3 gas for nonmalignant cells. In contrast, O_3 in ODM had

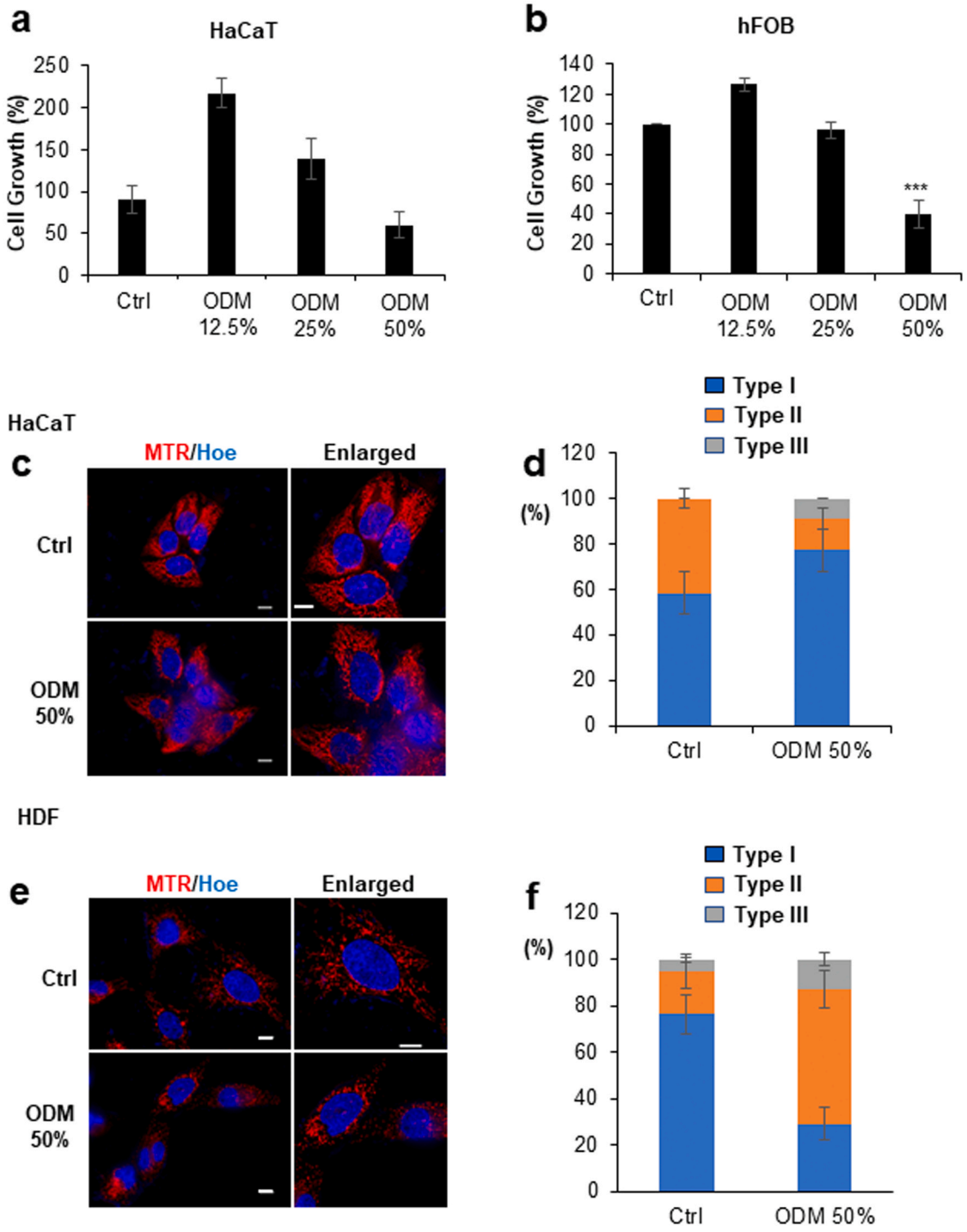

Fig. 9. ODM has low cytotoxicity in nonmalignant cells. (a, b) HaCaT (a) and hFOB (b) cells were treated with ODM at the indicated concentration for 72 h and were measured for viability by a WST-8 assay. Data were analyzed by own-way analysis of variance followed by Tuckey's post hoc test. * * $P < 0.01$; NS, not significant vs. control. (c, e) HaCaT (c) and HDFs (e) were treated with ODM (50%) for 2 h. After stimulation, cells were stained with MTR and Hoechst33342. Images were obtained and analyzed as described in the legend of Fig. 6. Scale bar = 10 μm. (d, f) Mitochondria exhibiting three different subcellular distributions (Type I, Type II, Type III) were counted in two or three pictures. Data are the mean ± SD (n = ~20).

little toxicity (Fig. 9). The report also demonstrated that O_3 gas caused mitochondrial permeability transition. However, our preliminary results showed that ODM had no such effect. A possible explanation for the discrepancies may be the different biological effects between O_3 gas and O_3 in solutions because O_3 in solutions can exhibit its physical impacts by acting in forms other than O_3, such as H_2O_2, $^{\bullet}OH$, and lipid oxides.

In summary, this study shows that O_3 in solutions can exhibit tumor-selective anticancer activity, primarily by triggering oxidative cell death independently of NOx. Mitochondrial oxidative stress and MPMC appear critical in effect. Our findings suggest that O_3 is a critical mediator of the action of APAM. ODM could be a chemically-defined instrument in cancer treatment.

Funding

This work was partly supported by JSPS KAKENHI, Grant Numbers

JP21K09217, and JP21K10128.

CrediT authorship contribution statement

Manami Suzuki-Karasaki: Investigation, Data acquisition, Formal analysis, Funding acquisition, Visualization, Writing – original draft, Writing – review & editing. **Yushi Ochiai:** Investigation, Data acquisition, Formal analysis. **Shizuka Innami:** Conceptualization, Investigation, Data acquisition, Formal analysis, Methodology, Resources. **Hiroshi Okajima:** Conceptualization, Investigation, Data acquisition, Formal analysis, Methodology, Resources, Project administration. **Miki Suzuki-Karasaki:** Investigation, Data acquisition, Formal analysis, Methodology, Resources. **Hideki Nakayama:** Project administration, Writing – review & editing, Supervision. **Yoshihiro Suzuki-Karasaki:** Conceptualization, Funding acquisition, Visualization, Project administration, Writing – original draft preparation, Writing – review & editing, Supervision.

Declaration of Competing Interest

Manami Suzuki-Karasaki, Miki Suzuki-Karasaki, and Yoshihiro Suzuki-Karasaki are working for the Private Research and Development Agency Plasma ChemiBio Laboratories. Hiroshi Okajima is working for Tokyo Keiki Incorp. Other authors have no conflicts of interest. The funders had no role in the study's design, in the collection, analyses, or interpretation of data, in the writing of the manuscript, or in the decision to publish the results.

Data Availability

Data will be made available on request.

Acknowledgments

We thank Dr. T Ando, the JCRB Cell Bank of the National Institutes of Biomedical Innovation, Health, and Nutrition (Osaka, Japan), and the Riken BioResource Center (Tsukuba, Japan) for providing cell lines.

Appendix A. Supporting information

Supplementary data associated with this article can be found in the online version at doi:10.1016/j.ejcb.2023.151346.

References

Agarwal, S., Ganesh, S., 2020. Perinuclear mitochondrial clustering, increased ROS levels, and HIF1 are required for the activation of HSF1 by heat stress. J. Cell Sci. 133, jcs245589. https://doi.org/10.1242/jcs.245589.

Al-Mehdi, A.B., Pastukh, V.M., Swiger, B.M., et al., 2012. Perinuclear mitochondrial clustering creates an oxidant-rich nuclear domain required for hypoxia-induced transcription. ([(DOI:)). Sci. Signal 5 (231), ra47. https://doi.org/10.1126/scisignal.2002712.

Ando, T., Suzuki-Karasaki, M., Ichikawa, J., et al., 2021. Combined anticancer effect of plasma-activated infusion and salinomycin by targeting autophagy and mitochondrial morphology ([(DOI:)). Front. Oncol. https//doi.org/10.3389/fonc.2021.593127.

Baeza-Noci, J., Pinto-Bonilla, R., 2021. Systemic review: ozone: a potential new chemotherapy ([(DOI:)). Int. J. Mol. Sci. 22, 11796. https://doi.org/10.3390/ijms222111796.

Bauer, G., 2019. The synergistic effect between hydrogen peroxide and nitrite, two long-lived molecular species from cold atmospheric plasma, triggers tumor cells to induce their cell death ([(DOI:)). Redox Biol., 101291. https://doi.org/10.1016/j.redox.2019.101291.

Bocci, V.A., 2006. Scientific and medical aspects of ozone therapy. State of the art ([(DOI:)). Arch. Med. Res. 37, 425–435. https://doi.org/10.1016/j.arcmed.2005.08.006.

Cannizzaro, A., Verga Falzacappa, C.V., Martinelli, M., et al., 2007. O(2/3) exposure inhibits cell progression affecting cyclin B1/cdk1 activity in SK-N-SH while induces Apoptosis in SK-N-DZ neuroblastoma cells. J. Cell Physiol. 213 (1), 115–125. https://doi.org/10.1002/jcp.21097].

Clavo, B., Santana-Rodríguez, N., Llontop, P., et al., 2018. Ozone therapy as adjuvant for cancer treatment: is further research warranted? ([(DOI:)). Evid. Based Complement Altern. Med. 2018, 7931849. https://doi.org/10.1155/2018/7931849.

Dixon, S.J., Stockwell, B.R., 2014. The role of iron and reactive oxygen species in cell death ([(DOI:)). Nat. Chem. Biol. 10, 9–17. https://doi.org/10.1038/nchembio.1416.

Forman, H.J., Kim, E., 1989. Inhibition by linoleic acid hydroperoxide of alveolar macrophage superoxide production: effects upon mitochondrial and plasma membrane potentials. ([(DOI:)). Arch. Biochem. Biophys. 274, 443–452. doi.org/10.1016/0003-9861(89)90457-8.

Girard, P.M., Arbabian, A., Fleury, M., et al., 2016. Synergistic effect of H2O2 and NO2 in cell death induced by cold atmospheric He plasma. Sci. Rep. 6:29098 https//doi.org/10.1038/srep29098.

Hassannia, B., Vandenabeele, P., Berghe, T.V., 2019. Targeting ferroptosis to iron out cancer. Cancer Cell 35, 830–849. https://doi.org/10.1016/j.ccell.2019.04.002.

Hirayama, T., Kadota, S., Niwa, M., Nakagawa, H., 2018. A mitochondria-targeted fluorescent probe for selective detection of mitochondrial labile Fe(II) ([(DOI:)). Metallomics 10, 794–801. https://doi.org/10.1039/c8mt00049b.

Hirayama, T., Okuda, K., Nakagawa, H., n.d. A highly selective turn-on fluorescent probe for iron(ii) to visualize labile iron in living cells. [(DOI:) Chem. Sci. 41250–41256. doi:org/⟨10.1039/C2SC21649C⟩].

Hoppins, S., Nunnari, J., 2012. Cell Biology. Mitochondrial dynamics and apoptosis-the ER connection ([(DOI:)). Science 337, 1052–1054. https://doi.org/10.1126/science.1224709.

Inoue, T., Suzuki, Y., 2013. Mitochondrial superoxide mediates mitochondrial and endoplasmic reticulum dysfunctions in TRAIL-induced apoptosis in Jurkat cells. Free Radic. Biol. Med. 61, 273–284. https://doi.org/10.1016/j.freeradbiomed.2013.04.020.

Ito, T., Ando, T., Suzuki-Karasaki, M., et al., 2018. Cold PSM, but not TRAIL, triggers autophagic cell death: a therapeutic advantage of PSM over TRAIL. 2018;53(2):503-14. DOI:) Int. J. Oncol. 53, 503–514 https//doi.org/10.3892/ijo.2018.4413.

Jiang, H., Wang, H., De Ridder, M., 2018. Targeting antioxidant enzymes as a radiosensitizing strategy. DOI:) Cancer Lett. 438, 154–164. https://doi.org/10.1016/j.canlet.2018.09.004.

Jo, A., Bae, J.H., Yoon, Y.J., et al., 2022. Plasma-activated medium induces ferroptosis by depleting FSP1 in human lung cancer cells ([(DOI:)). Cell Death Dis. 13, 212. https//doi.org/10.1038/s41419-022-04660-9.

Kamm, A., Przychodzen, P., Kuban-Jankowska, A., et al., 2019. Nitric oxide and its derivatives in the cancer battlefield ([(DOI:)). Nitric Oxide 93, 102–114. https://doi.org/10.1016/j.niox.2019.09.005.

Keidar, Walk, M., Shashurin, R., et al., 2012. Cold plasma selectivity and the possibility of a paradigm shift in cancer therapy ([DOI:). Br. J. Cancer 105, 1295–1301. https//doi.org/10.1038/bjc.2011.386.

Kim, J., Thomas, S.N., 2022. Opportunities for nitric oxide in potentiating cancer immunotherapy ([DOI:). Pharmacol. Rev. 74, 1146–1175. https://doi.org/10.1124/pharmrev.121.000500.

Lunov, O., Zablotskii, V., Churpita, O., et al., 2014. Cell death induced by ozone and various non-thermal plasmas: therapeutic perspectives and limitations ([DOI:). Sci. Rep. 4, 7129. https://doi.org/10.1038/srep07129.

Lunov, O., Zablotskii, V., Churpita, O., et al., 2017. Chemically different non-thermal plasmas target distinct cell death pathways ([DOI:). Sci. Rep. 7, 600. https://doi.org/10.1038/s41598-017-00689-5.

Meister, A., 1995. Mitochondrial changes associated with glutathione deficiency ([DOI:). Biochim Biophys. Acta 1271, 35–42. https://doi.org/10.1016/0925-4439(95)00007-q.

Mokhtari, H., Farahmand, L., Yaserian, K., Jalili, N., Majidzadeh-A, K., 2019. The antiproliferative effects of cold atmospheric plasma-activated media on different cancer cell lines, the implication of ozone as a possible underlying mechanism ([DOI:). J. Cell Physiol. 234, 6778–6782. https://doi.org/10.1002/jcp.27428.

Pedriali, G., Rimessi, A., Sbano, L., et al., 2017. Regulation of endoplasmic reticulum-mitochondria Ca ([DOI:). Front. Oncol. 7, 180. https://doi.org/10.3389/fonc.2017.00180.

Pendin, D., Filadi, R., Pizzo, P., 2017. The concerted action of mitochondrial dynamics and positioning: new characters in cancer onset and progression ([DOI:). Front. Oncol. 7, 102. https://doi.org/10.3389/fonc.201, 7.00102.

Quintana, A., Schwarz, E.C., Schwindling, C., et al., 2006. Sustained activity of calcium release-activated calcium channels requires translocation of mitochondria to the plasma membrane ([DOI:). J. Biol. Chem. 281, 40302–40309. https://doi.org/10.1074/jbc.M607896200.

Saito, K., Asai, T., Fujiwara, K., et al. Tumor-selective mitochondrial network collapse induced by atmospheric gas plasma-activated medium. ([DOI:) Oncotarget. 7: 19910–19927. doi.org/ 10.18632/oncotarget.7889].

Simonetti, V., Quagliariello, V., Giustetto, P., Franzini, M., Iaffaioli, R.V., 2017. Association of ozone with 5-fluorouracil and cisplatin in regulation of human colon cancer cell viability: in vitro anti-inflammatory properties of ozone in colon cancer cells exposed to lipopolysaccharides ([DOI:). Evid. Based Complement Altern. Med. 2017, 7414083. https://doi.org/10.1155/2017/7414083.

Stockwell, B.R., 2022. Ferroptosis turns 10: emerging mechanisms, physiological functions, and therapeutic applications ([DOI:). Cell 185 (14), 2401–2421. https://doi.org/10.1016/j.cell.2022.06.003.

Suzuki, Y., Inoue, T., Murai, M., et al., 2012. Depolarization potentiates TRAIL-induced Apoptosis in human melanoma cells: role for ATP-sensitive K+ channels and endoplasmic reticulum stress ([DOI:). Int. J. Oncol. 41, 465–475. https://doi.org/10.3892/ijo.2012.1483.

Suzuki-Karasaki, M., Ando, T., Ochiai, Y., et al., 2022. Air plasma-activated medium evokes a death-associated perinuclear mitochondrial clustering ([DOI:). Int. J. Mol. Sci. 23, 1124. https://doi.org/10.3390/ijms23031124.

Suzuki-Karasaki, Y., Fujiwara, K., Saito, K., et al., 2015. Distinct effects of TRAIL on the mitochondrial network in human cancer cells and normal cells: role of plasma membrane depolarization ([DOI:). Oncotarget 6, 21572–21588. https://doi.org/10.18632/oncotarget.4268.

Twig, G., Shirihai, O.S., 2011. The interplay between mitochondrial dynamics and mitophagy ([DOI:). Antioxid. Redox Signal. 14, 1939–1951. https://doi.org/10.1089/ars.2010.3779.

Yan, D., Sherman, J.H., Keidar, M., 2018. The application of the cold atmospheric plasma-activated solutions in cancer treatment ([DOI:] Anticancer Agents Med. Chem. 18, 769–775. https//doi.org/10.2174/1871520617666170731115233.

Yoshikawa, N., Liu, W., Nakamura, K., et al., 2020. Plasma-activated medium promotes autophagic cell death along with alteration of the mTOR pathway ([DOI:] Sci. Rep. 10, 1614. https//doi.org/10.1038/s41598-020-58667-3.

Zänker, K.S., Kroczek, R., 1990. In vitro synergistic activity of 5-fluorouracil with low-dose ozone against a chemoresistant tumor cell line and fresh human tumor cells ([DOI:] Chemotherapy 36, 147–154. https://doi.org/10.1159/000238761.

Update

European Journal of Cell Biology
Volume 103, Issue 1, March 2024, Page

DOI: https://doi.org/10.1016/j.ejcb.2024.151385

European Journal of Cell Biology 103 (2024) 151385

Contents lists available at ScienceDirect

European Journal of Cell Biology

journal homepage: www.elsevier.com/locate/ejcb

Corrigendum

Corrigendum to "Ozone mediates the anticancer effect of air plasma by triggering oxidative cell death caused by H_2O_2 and iron" [Eur. J. Cell Biol. 102 (2023) 151346]

M. Suzuki-Karasaki [a,b], Y. Ochiai [a], S. Innami [a], H. Okajima [c], H. Nakayama [d], Y. Suzuki-Karasaki [a,*]

[a] Department of Research and Development, Plasma ChemiBio Laboratory, Nasushiobara, Tochigi, Japan
[b] Graduate School of Medical Sciences, Kumamoto University, Kumamoto, Japan
[c] Communication & Control Systems Company, Tokyo Keiki Incorporation, Tokyo, Japan
[d] Department of Oral and Maxillofacial Surgery, Faculty of Life Sciences, Kumamoto University, Kumamoto, Japan

The authors regret < In Fig-7(e), the top panel MTR/Hoe image of control (Ctrl) was incorrectly shown in the original article. The correct image is as below.>

The authors would like to apologize for any inconvenience caused.

Page /Cell	Incorrect	Correct
Fig7-(e)/143B	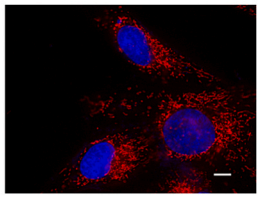	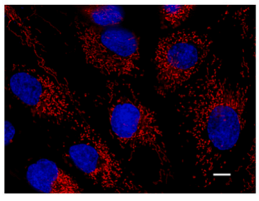

DOI of original article: https://doi.org/10.1016/j.ejcb.2023.151346.
* Corresponding author.
E-mail address: Suzuki.pcbl@gmail.com (Y. Suzuki-Karasaki).

https://doi.org/10.1016/j.ejcb.2024.151385

Available online 15 January 2024